Stereoisomers of oxime ethers of 1,4-naphthoquinone: Synthesis, characterization, X-ray crystal structures, and DFT studies

Vivek Mokashi[a], Sunita Salunke-Gawali[a]*, Maneesha Shewale[b], Shridhar P. Gejji[a], Ray J. Butcher[c]

[a]*Department of Chemistry, Savitribai Phule Pune University, Pune 411007, Maharashtra, India*

[b]*Department of Chemistry, Baburaoji Gholap College, Sangvi, Pune-411027, Maharashtra, India*

[c]*Department of Chemistry, Howard University, Washington, D.C, 20059, USA*

E-mail: sunita.salunke@unipune.ac.in

Abstract

In the present work, we use the C-3 substituted 2-hydroxy-1,4-naphthoquinones viz. 2-hydroxynaphthalene-1,4-dione (**1**), 2-hydroxy-3-methylnaphthalene-1,4-dione (**2**), and 2-chloro-3-hydroxynaphthalene-1,4-dione (**3**) as starting materials and obtained naphthoquinoneoxime ethers *viz.* 3-hydroxy-4-(methoxyimino)naphthalen-1(4H)-one (**4**), 3-hydroxy-4-(methoxyimino)-2-methylnaphthalen-1(4H)-one (**5**) and 2-chloro-3-hydroxy-4-(methoxyimino)naphthalen-1(4H)-one (**6**) *via* a facile and efficient synthesis involving condensation with methoxyamine hydrochloride. X-ray structure showed that **4** belongs to the orthorhombic ($P2_12_12_1$) space group, whereas **5** and **6** ($P2_1/c$) crystalize in the monoclinic crystal system. The isomer ratios derived from NMR experiments elucidating stereoisomerism in compounds comprised of carbon-nitrogen double bonds have been analyzed; the naphthoquinone oxime ethers **4**, **5**, and **6** were also characterized employing the ωB97x-D/6-311++G (d, p) level of density functional theory. Theoretical studies reveal different conformational isomers with the '*amphi'* and '*syn'* isomers as low-lying structures along their energy hierarchy in accordance with the X-ray crystallography data**.** The spectral

characterization of vibrational frequencies and ^{1}H /^{13}C NMR chemical shifts in unison with experiments and theory has been presented.

Key Words: stereoisomers, naphthoquinoneoxime, naphthoquinone, hydrogen bonding, DFT

1. Introduction

Oxime-based ligands are crucial in several areas of chemistry and are extensively used in analytical chemistry to separate or detect metal ions. For example, dimethylglyoxime is a common oxime-based ligand used in gravimetric Ni(II) determination. In industry, phenolic oximes are widely used for copper extraction[1]. Rane et al. [2] discussed *syn, anti,* and *amphi* stereoisomers of naphthoquinone monooximes. Percentages of the conformational isomers were then derived, exploring the integration method in the ^{1}H NMR spectroscopy. The formation and stability of their various forms were found to be dependent on quinone moiety and its structural features. Our research group identified *ortho* and *para* tautomerism in 2-hydroxy-1,4-naphthoqunone-1-oxime [3-5] and o-hydroxyanilino-1,4-naphthoquinone [6] derivatives, which are HPLC separated; the accompanying tautomeric interconversion was subsequently investigated through time-dependent NMR studies. Theoretical works by Gejji et al. on 2-hydroxy-3-methyl-1,4-naphthoquinone-1-oxime employing the HF and H3LYP density functional methods [7] showed that it exists predominantly in the *amphi* form.

Oxime and oxime ether constitute functional groups of oxygen linked to imine nitrogen. Oxime ether-containing compounds are renowned for their diverse and rich chemistry. Such oxime ether functionalities provide desirable options in the drug designing of various pharmaceutical agents partly due to their relatively simple synthesis and remarkable medicinal chemistry applications. The oxime ether group serves as a vital medicinal motif and is present in numerous pharmaceutically active compounds widely explored in various pesticides. For example, fenpyroximate is an oxime ether-containing pesticide extensively used worldwide and shown to be highly effective against acaricides [8]. Chattopadhyay et al. reported that the

thioaryl naphthylmethanone oxime ether derivative demonstrated remarkable anticancer properties for various cancer cells[9]. Notably, their presence in different medicinal scaffolds renders them with a wide range of biological and pharmaceutical properties, including antibacterial [10-12] and antifungal [13-15]. Anti-inflammatory [16-17], antitumor[18-19], and anti-protozoan[20], the oxime ether group thus is considered to be a privileged group in Chemistry, and therefore, the oxime ether group; their structures and reactivity are the focus of attention for quite some years [21-24]. The oxime ether group with the presence of the C=N group and how it renders isomerism have been investigated from theoretical perspectives in the literature [25-27]. Stereoisomers possess different physical and chemical properties, with the physiochemical properties showing a strong dependence on the types and number of atoms within a molecule. Besides, the spatial arrangement is essential in governing the physiochemical properties, and the binding from the particular receptor originates from different spatial arrangements. The isomers, therefore, exhibit diverse biological and toxicological effects [28-29]. For this reason, knowledge of isomerism is considered necessary in designing and developing drugs that are primarily potent and less toxic. In this light, we focus on synthesis and isomerism in new naphthoquinone oxime ether derivatives in the present investigation, characterized by their structural features and spectroscopic properties.

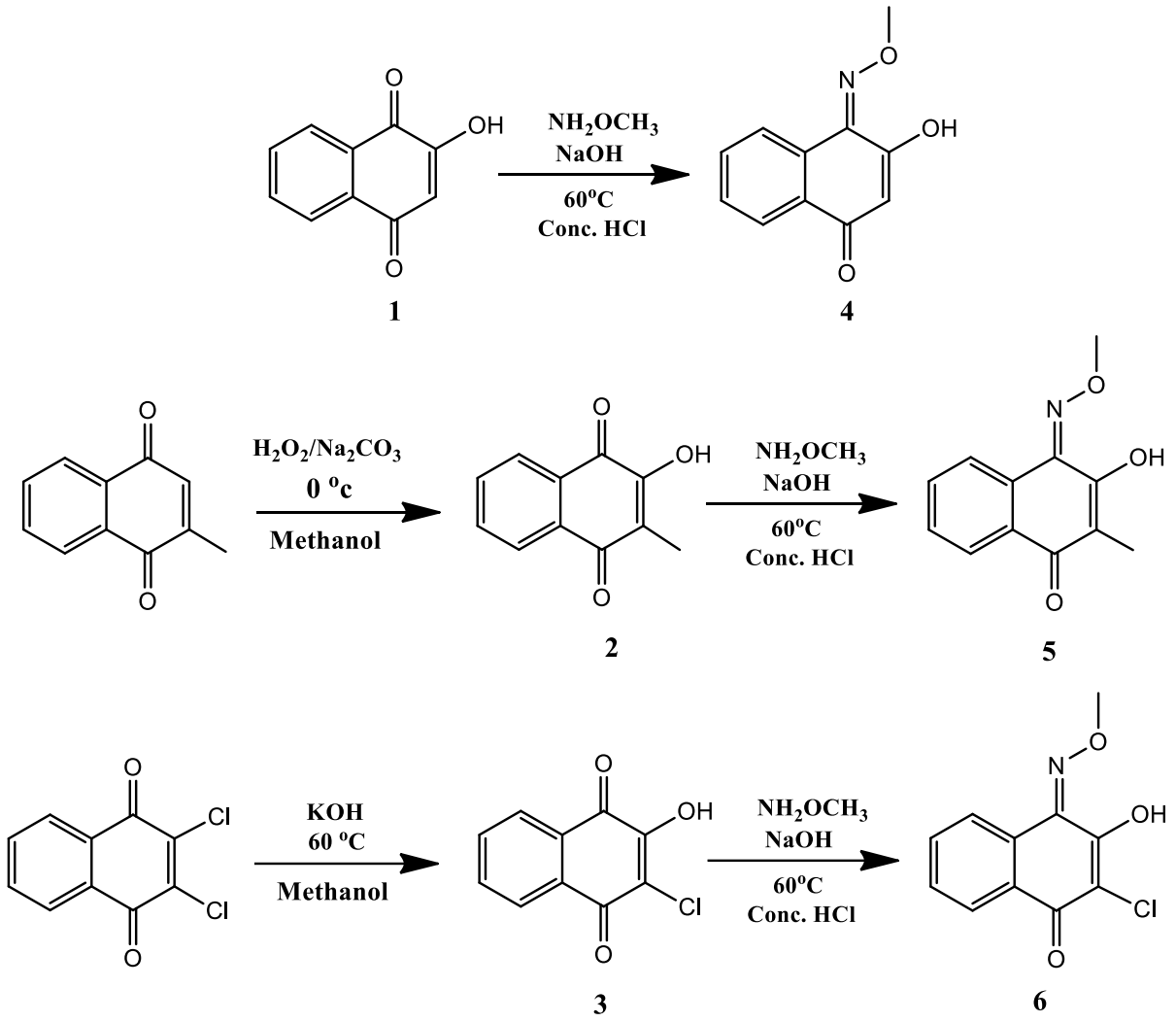

Scheme 1 Synthetic pathway for naphthoquinone oxime ether derivatives.

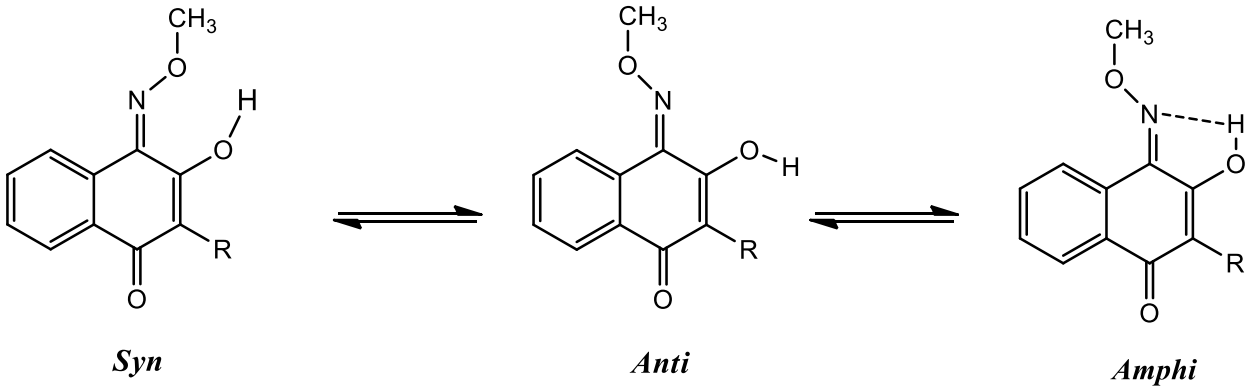

Fig. 1. Various stereoisomers of naphthoquinone oxime ether**.**

2. Experimental

2.1. General materials and methods

The chemicals used viz 2-hydroxynaphthalene-1,4-dione, 2-methylnaphthalene-1,4-dione, 2,3-dichloronaphthalene-1,4-dione, methoxyamine hydrochloride, and was obtained from Sigma Aldrich. Sodium carbonate (Na_2CO_3), Ammonium bicarbonate (NH_4HCO_3), Sodium hydroxide (NaOH), Potassium hydroxide (KOH), conc. HCl, conc. H_2SO_4 was purchased from Qualigen Chemicals. HPLC grade Acetonitrile, AR grade DMSO, AR grade methanol, diethyl ether, and Hydrogen Peroxide (H_2O_2) were obtained from Merck Chemicals. Milli Q water is used wherever necessary.

The infrared spectra were recorded on Bruker Tenor 37 (ATR) spectrophotometer in the solid state between 4000 cm^{-1} to 400 cm^{-1} (Fig.S1 to Fig.S3 in ESI†). ^{1}H, ^{13}C, HSQC, and COSY NMR were recorded on Bruker NMR spectrometer (400 MHz and 100 MHz) in DMSO-d_6 using TMS as an internal reference (Fig.S4 to Fig.S15 in ESI†) chemical shift values presented in ppm, with splitting patterns denoted as s (singlet), d (doublet), t (triplet), q (quartet), dd (doublet of doublet), and m (multiplet). The UV-visible spectra were recorded in DMSO on the Shimadzu UV 1800 spectrophotometer (Fig.S16 of ESI†). MALDI time of flight (TOF) spectra were recorded on MALDI-TOF-Mass spectroscopy 4800 (Fig S17 to Fig S19 in ESI†), Shimadzu Prominence LC-20AD liquid chromatogram has been used to separate isomers, and SPD-20A UV/VIS detector was employed with a manual injection system, connected with LC solution with a multiple channel module. 2-hydroxy-3-methylnaphthalene-1,4-dione (**2**) and 2-chloro-3-hydroxynaphthalene-1,4-dione (**3**) were synthesized using previously reported methods [30-31] (Scheme 1).

The Agilent Eclipse plus C 18 column [length=100 mm, internal diameter=4.6 mm, particle size=3.5 µm, pore size=95 Å] has been used to separate isomers. The mobile phase, consisting of ammonium bicarbonate and acetonitrile, was used in various proportions. The detector was set at 254 nm. The detailed chromatographic conditions used for isomer separation are mentioned in the supplementary information (Fig.S20 in ESI†).

*2.2. General synthetic procedure for **4, 5** and **6***

The following procedure was used to synthesize oxime ether derivatives **4**, **5**, and **6** from precursors **1**, **2**, and **3**, respectively (Scheme 1). To the solution of 0.5 g (2.87 mmol of **1** for **4**, 2.65 mmol of **2** for **5**, and 2.39 mmol of **3** for **6**) in 30 ml 2N, NaOH, 5 ml aqueous solution of methoxy amine hydrochloride (4.30 mmol for **4**, 3.97 mmol for **5** and 3.59 mmol for **6**) was added. The mixture was magnetically stirred and heated at 60°C for 2 hours. The reaction mixture was cooled and neutralized with 2N conc. HCl. After neutralizing, a yellow-colored precipitate was obtained. It was filtered, washed with cold water, and dried in a vacuum to get naphthoquinone oxime ethers **4**, **5**, and **6**. During the execution of an independent experiment related to synthesizing the copper complex **5**, yellow crystals of '*syn'* isomer were obtained in the filtrate as an unreacted starting material; they are designated as **5b***.

*2.3. Characterization of 3-hydroxy-4-(methoxyimino)naphthalen-1(4H)-one (**4**)*

Yellow solid, yield: 0.55g (95 %); FT-IR (ATR): ν(cm^{-1}) = 3296, 2955, 1660, 1641, 1592, 1571, 1460, 1385, 1344, 1325, 1287, 1187, 1158, 1026, 901, 823, 774, 699, 586. ^{1}H NMR (400 MHz, DMSO-d_6, δ (ppm)): 4.17 (*amphi*), 4.26 (*syn*) (3H, s, N-OCH_3), 5.88 (*amphi*), 5.93 (*syn*) (1H, s, allylic hydrogen), 7.56-7.70 (2H, m, Ar-H), 8.05 (1H, d, J = 6.4 Hz, Ar-H), 8.76 (1H, d, J= 7.2 Hz, Ar-H), 11.07 (*amphi*), 11.29 (*syn*) (1H, s, O-H). ^{13}C NMR (100 MHz, DMSO-d_6, δ (ppm)): 65.32, 106.39, 108.63, 123.78, 125.10, 126.13, 126.89, 129.98, 130.41, 131.32, 132.09, 132.89, 141.45. 163.87, 184.04. UV-Vis; (λ_{max}(nm), DMSO): 296, 339. MALDI-TOF/TOF: Calc. For $[C_{11}H_9NO_3+H]^+$ *m/z* 204.07, Found *m/z* 204.55.

*2.4. Characterization of 3-hydroxy-4-(methoxyimino)-2-methylnaphthalen-1(4H)-one (**5**)*

Yellow solid, yield: 0.55 g (96 %); FT-IR (ATR): ν (cm^{-1}): 3328, 2942, 1658, 1633, 1591, 1572, 1551, 1459, 1376, 1354, 1277, 1189, 1028, 897, 844, 775, 684, 568. ^{1}H NMR (400 MHz, DMSO-d_6, δ (ppm)): 1.91 (*amphi*), 1.94 (*syn*) (3H, s, -CH_3), 4.20 (*amphi*), 4.28 (*syn*) (3H, s, -

OC<u>H</u>$_3$), 7.66 (1H, m, Ar-H), 7.81 (1H, m, Ar-H), 7.99 (1H, t, *J* = 8.4 Hz Ar-H), 8.74 (1H, d, *J*= 7.6 Hz, Ar-H), 10.03 (*amphi*), 10.95 (*syn*) (1H, s, O-H). ^{13}C NMR (100 MHz, DMSO-d_6, δ (ppm)): 8.88, 9.03, 65.26, 65.46, 120.41, 123.36, 126.12, 129.97, 132.49, 133.58, 134.88, 155.98, 158.01, 181.17, 185.18. UV-Vis; (λ_{max}(nm), DMSO): 306, 334. MALDI-TOF/TOF: Calc. For $[C_{12}H_{11}NO_3+H]^+$ *m/z* 218.07, Found *m/z* 218.60.

2.5. Characterization of *2-chloro-3-hydroxy-4-(methoxyimino)naphthalen-1(4H)-one* (**6**)

Yellow solid, yield: 0.53 g (94 %); FT-IR (ATR): *v* (cm^{-1}): 3268, 2940, 1633, 1559, 1452, 1368, 1325, 1271, 1201, 1031, 893, 850, 720, 680. ^{1}H NMR (400 MHz, DMSO-d_6, δ (ppm)): 4.22 (*amphi*), 4.32 (*syn*) (3H, s, O-CH$_3$), 7.44 (2H, m, Ar-H), 7.99 (1H, dd, *J* = 7.6 Hz, *J* = 7.8 Hz, Ar-H), 8.12 (1H, d, *J* = 7.6 Hz, Ar-H), 8.75 (1H, d, *J* = 8 Hz Ar-H). ^{13}C NMR (100 MHz, DMSO-d_6, δ (ppm)): 65.21, 65.90, 111.71, 115.65, 123.72, 125.44, 125.99, 126.92, 129.08, 130.17, 130.53, 131.70, 133.46, 135.89, 140.46, 140.82, 155.74, 158.97, 176.26, 177.59. UV-Vis; (λ_{max}(nm), DMSO): 296, 339. MALDI-TOF/TOF: Calc. For $[C_{11}H_8\ ClNO_3+H]^+$ *m/z* 238.03, Found *m/z* 238.09.

2.6. X-ray crystallographic data collection and refinement of structures for **4**, **5**, *and* **6**

X-ray quality crystals of **4, 5,** and **6** were harvested after slow evaporation of the methanol. The crystals of appropriate size were chosen for data collection. The data for **4** and **6** was collected on a D8 venture PHOTON 100 CMOS diffractometer using graphite monochromated MoKα radiation (λ = 0.71073 Å) from a Mo-target rotating-anode X-ray source (for **5b***, MoKα radiation (λ = 1.54184 Å)). Final cell constants were obtained from the least-squares fit of several thousand strong reflections. Intensity data were corrected for absorption using intensities of redundant reflection with the program SADABS [32]. The structures were solved readily by direct method and subsequent difference Fourier techniques. The Siemens SHELXTL software package was used for the structure's solution and artwork; SHELXL 2018/3, based on F^2, was used to refine the structures [33]. All non-hydrogen atoms were anisotropically refined, and hydrogen atoms were placed at the calculated position and refined as riding atoms with isotropic displacement parameters. The crystal packing diagrams (Fig.4 to Fig.7) were drawn using Mercury 3.8 software. The π-π stacking distances were obtained from this software.

Data of **5** was collected on the ChemMatCARS Sector 15 beamline at the Advanced Photon Source. The crystal was mounted on a fine glass fiber, and data was collected at a wavelength of 0.41328 Å on a Huber goniometer equipped with a Dectris active pixel detector.

2.7. Computational Details

Different conformation isomers of **4**, **5**, and **6** were generated varying spatial orientations of hydroxyl and the methoxy groups. These were optimized using the GAUSSIAN-16 suite of programs [34]. We employ the hybrid ωB97x-D exchange-correlation functional-based density functional theory in conjunction with the internally stored 6-311++G(d, p) basis set incorporating polarized and diffuse functions on all-atom centers in

these isomers. The appraisal of charge distribution in these systems was carried out through the frontier molecular orbitals computed from theory. The computed expected vibration frequencies confirm the stationary point structures as local minima on multivariate potential energy surfaces. The GAUSSVIEW-6 program was utilized for acuminous visualization. Furthermore, the ^{1}H NMR chemical shifts (δ_H) were calculated by subtracting the nuclear magnetic shielding tensors of protons in isomers from those in tetramethylsilane (reference) using the gauge-independent atomic orbital (GIAO) theory [35]. The effect of solvation on relative stabilization energies was simulated through the self-consistent reaction field (SCRF) theory incorporating the polarizable continuum model (PCM) [36].

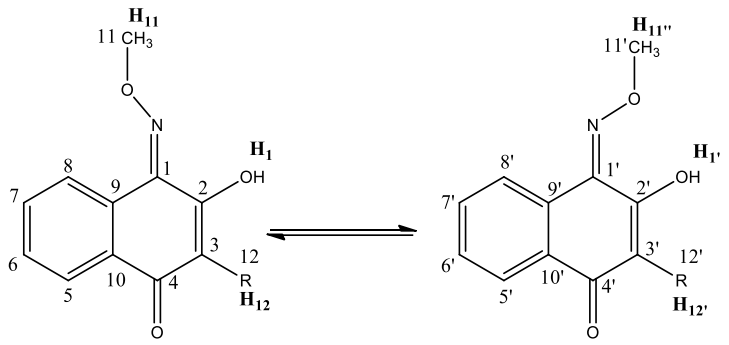

Amphi ***Syn***

Compound	R	*Amphi* isomer	*Syn* isomer
4	H	**4**a	**4**b
5	CH_3	**5**a	**5**b
6	Cl	**6**a	**6**b

Fig. 2. Two equilibrating isomers of **4**, **5**, and **6**.

3. Result and Discussion

3.1. Synthesis and characterization of **4**, **5** *and* **6**

The precursors **2** and **3** were synthesized according to the reported procedure. Reactions **1**, **2**, and **3** with methoxy amine hydrochloride led to the formation of desired naphthoquinone oxime ether derivatives **4**, **5**, and **6** (Scheme 1). It is essential to note that naphthoquinone oxime ether derivatives **4**, **5**, and **6** were obtained as a mixture of stereoisomers. The

stereochemistry of hydroxy naphthoquinone oximes is well studied[2, 37], where '*syn'* and '*anti'* forms are stereoisomers while the '*amphi'* form conforms to the '*anti'* isomer. Similar types of isomerism were also observed in **4**, **5**, and **6,** shown in Fig.1.

The structure elucidation of newly synthesized compounds was carried out using a variety of experimental techniques such as ^{1}H NMR (Fig.S4, Fig.S6, Fig.S8 in ESI†) ^{13}C NMR (Fig.S5, Fig.S7, Fig.S9 in ESI†), COSY (Fig.S10, Fig.S12, Fig.S14 in ESI†), HSQC (Fig.S11, Fig.S13, Fig.S15 in ESI†), FT-IR (Fig.S1 through Fig.S3 in ESI†), UV-Visible spectroscopy (Fig.S16 in ESI†), MALDI (Fig.S17 through Fig.S19 in ESI†), in combination single X-ray diffraction studies (Fig.S21 through Fig.S28 ESI†) and Theoretical DFT studies. *Syn* and *amphi* isomers can convert into one other, and this conversion may occur based on several experimental conditions such as pH, solvation, and temperature. NMR Spectroscopy is a technique that is most frequently used to determine the *syn* and *anti*-isomers of compounds. In this study, ^{1}H NMR of synthesized compounds was taken, and the percentage of isomers was determined by integration values obtained from ^{1}H NMR data.

3.2. FT-IR, ^{1}H, ^{13}C NMR and UV-Visible studies

The FT-IR bands of synthesized compounds are assigned by comparing the frequencies observed with similar derivatives. The FT-IR spectra of **4**, **5**, and **6** (Fig. S1 through Fig. S3 of ESI†) revealed the presence of a band at ~3296, ~3328, and ~3268 cm^{-1} respectively was assigned to $\nu_{\text{-OH}}$ vibrations. The medium intensity bands around 2945 cm^{-1} in all three compounds attributed to stretching vibrations of the -CH_3 group. The absorption bands between 1559-1571 cm^{-1} are assigned to the $\nu_{C=N}$ stretch. Other important stretching frequencies are summarized in Table 1.

^{1}H and ^{13}C NMR of **4**, **5**, and **6** exhibit complex profiles because of isomers that may be present in the solution. The atoms are numbered in the same order as in Fig. 2. ^{1}H NMR of **5** shows two sets of proton signals; quite similar types of profiles were observed in ^{1}H NMR

of **4** and **6** (Fig. S4, Fig. S6, Fig. S8 in ESI†) which indicate the presence of isomers *syn*/*amphi* in solution. Table 2 describes the percentage of isomers obtained from integration values of ^{1}H NMR spectra of **4**, **5**, and **6**. However, the relative percentage of *syn* and *amphi* isomers was estimated from the integration of methoxy proton (-OCH_3) as this proton is a singlet and is present in all three derivatives. ^{1}H NMR of **5** shows two singlet signals at 1.91 and 1.94 ppm for hydrogens at different isomers. H(12) is attributed to *amphi* isomer whereas H(12') is for *syn* isomer (Fig. S6 in ESI†). Furthermore, two broad singlets at 10.03 and 10.95 ppm are ascribed to H(1) and H(1') hydroxyl protons; likewise, H(11) and H(11') are attributed to methoxy protons. *Amphi* isomers were predominant in all three molecules, probably due to less molecular crowding than *syn* isomers. In the ^{13}C NMR spectrum of **4**, **5,** and **6**, some duplicate signals were noticed (Fig.S5, Fig.S7, and Fig.S9 in ESI†), ^{13}C NMR of **5** (Fig.S7 in ESI†) showed a signal at 141.54 and 140.22 ppm corresponding to carbon C(1) and C(1)' of respective stereoisomer. The methoxy carbon (-OCH_3) C(11) and C(11')(Fig.S7 in ESI†) in compound **5** appear at 65.26 and 65.46 for *amphi* and *syn* isomers respectively.

UV-visible spectra (Fig. S16 in ESI†) of synthesized compounds **4**, **5**, and **6** were investigated at room temperature in DMSO with 10^{-5} M concentration. The literature report on closely related compounds assigns the UV-visible absorption bands [22, 38]. The UV-visible absorption spectra of **4**, **5**, and **6** exhibited two expected bands at 290±10 nm and 330± 20 nm regions mainly arising due to $\pi \rightarrow \pi^*$ electronic transitions.

Table 1 Experimental and optimized vibrational frequencies (ν in cm^{-1}) of **4**, **5**, and **6**.

Compound	Stretching		ν(O-H)	ν(OC-H)	ν(C=O)	ν(C=N)	ν(C-O)	ν(C-Cl)
4	Theoretical	**4a** (*Amphi*)	3490	2860	1659	1583	1175	-
		4b (*Syn*)	3504	2867	1660	1563	1176	-
	Experimental		3296	2955	1660	1571	1187	-
5	Theoretical	**5a** (*Amphi*)	3486	2857	1652	1587	1169	-
		5b (*Syn*)	3503	2865	1652	1564	1188	-
	Experimental		3328	2942	1658	1572	1189	-
6	Theoretical	**6a** (*Amphi*)	3476	2861	1659	1583	1175	636
		6b (*Syn*)	3483	2867	1673	1558	1342	825
	Experimental		3268	2940	1633	1559	1203	680

Table 2 shows the Assignment of ^{1}H NMR signals (in ppm) and *the syn*/*amphi* isomer ratios of **4**, **5,** and **6**.

Compound	δ (ppm) H(3)/H(3)'	δ (ppm) H(11)/H(11')	δ (ppm) H(1)/H(1')	*% (Amphi/Syn)*
4	5.88/5.93	4.17/4.26	11.08/11.28	58:42
5	-	4.20/4.28	10.03/10.95	53:47
6	-	4.22/4.32	-	60:40

3.3. Single crystal X-ray diffraction Studies

Table 3 Single Crystal X-ray data for **4**, **5**, **5b***and **6**

Identification code	**4**	**5**	**5b***	**6**
CCDC No	2298742	2298744	2329132	2298743
Empirical formula	$C_{11}H_9NO_3$	$C_{12}H_{11}NO_3$	$C_{12}H_{11}NO_3$	$C_{11}H_8ClNO_3$
Formula weight	203.19	217.22	217.22	237.63
Temperature	298(2) K	100(2) K	100(2) K	100(2) K
Wavelength	0.71073 Å	0.41328 Å	1.54184 Å	0.71073 Å
Crystal system, space group	Orthorhombic, $P2_12_12_1$	Monoclinic, $P2_{1/c}$	Monoclinic, $P2_{1/c}$	Monoclinic, $P2_{1/c}$
Unit cell dimensions	a = 3.9212(6)Å, b = 13.366(8) Å c = 18.145(3)	a = 13.883(6) Å b = 3.8754(16) Å β = 97.608(8)° c = 18.898(8) Å	a = 9.6818(2) Å b = 16.8169(4) Å, β = 106.456(3)° c = 12.8540(4) Å	a = 4.69910(10) Å, b = 15.2192(4) Å β= 95.7050(10)° c = 14.2486(2) Å
Volume, Å^3	951.0(3)	1007.8(7)	2007.13(9)	1013.96(4)
Z, Calculated density	4, 1.419 Mg/m^3	4, 1.432 Mg/m^3	8, 1.438 Mg/m^3	4, 1.557 Mg/m^3
Absorption coefficient	0.105 mm^{-1}	0.042 mm^{-1}	0.865 mm^{-1}	0.366 mm^{-1}
F(000)	424	456	912	488
Theta range for data collection	2.245 to 26.390 °	0.632 to 14.966°	4.447 to 76.170°	1.963 to 36.370°
Limiting indices	-3 ≤ h ≤ 4, -16 ≤ k ≤ 16, -22 ≤ l ≤ 22	-17 ≤ h ≤ 17, -4 ≤ k ≤ 4, -23 ≤ l ≤ 23	-12<=h<=12, -20<=k<=20, -16<=l<=15	-5 ≤ h ≤7, -25 ≤ k ≤ 24, -23 ≤ l ≤23
Reflections collected / unique	17297 / 1937[R(int) = 0.0799]	25872 / 2062 [R(int) = 0.1325]	110814/ 4176 [R(int) = 0.2131]	46673 / 4668 [R(int) = 0.0421]
Completeness to theta = 25.242°	99.3 %	97.8%	100.0 %	97. 0%
Refinement method	Full-matrix least-squares on F^2	Full-matrix least-squares on F^2	Semi-empirical from equivalents	Full-matrix least-squares on F^2
Data/restraints/parameters	1937 / 72 / 168	2062 / 72 / 181	4176 / 0 / 299	4668 / 0 / 150
Goodness-of-fit on F^2	1.032	1.046	1.145	1.078
Final R indices [I > 2sigma(I)]	R_1 = 0.0397, wR_2 = 0.0797	R_1 = 0.0771, wR_2 = 0.2102	R1 = 0.0887, wR2 = 0.2103	R_1 = 0.0314, wR_2 = 0.0896
R indices (all data)	R_1 = 0.0498, wR_2 = 0.1040	R_1 = 0.1075, wR_2 = 0.2431	R1 = 0.0985, wR2 = 0.2169	R_1 = 0.0374, wR_2 = 0.0921
Extinction coefficient	n/a	0.06(3)	n/a	n/a
Largest diff. Peak and hole	0.131 and -0.127 e.Å^{-3}	0.718 and -0.629 e.Å^{-3}	0.624 and -0.336 e.Å^{-3}	0.388 and -0.468 e.Å^{-3}

Table 4 Selected bond distances and bond angles of **4**, **5** and **6**

Compound	Bond	Bond distance	∠	°
4	C(1)-N(1)# C(1)-N(1A) O(2)-C(4)# C(2)-O(1)# C(2)-C(3)# C(11)-O(3) # C(11A)-O(3A)	1.305(3) 1.35(2) 1.227(3) 1.353(3) 1.337(4) 1.433(4) 1.43(4)	C(1)-N(1)-O(3)# C(1)-N(1A)-O(3A) N(1)-O(3)-C(11)# N(1A)-O(3A)-C(11A) C(2)-O(1)-H(1O)#	112.7(2), 103.4(16) 109.9(2) 112.6(18) 109.5
5	N(1)-C(4), N(1A)-C(4)# O(1)-C(1) O(2)-C(3) O(3)-C(12), O(3A)-C(12A)# C(2)-C(3)	1.295(5) 1.51(7) 1.232(4) 1.363(4) 1.450(6) 1.38(8) 1.347(5)	C(4)-N(1)-O(3) O(3A)-N(1A)-C(4)# N(1)-O(3)-C(12) N(1A)-O(3A)-C(12A)# C(3)-O(2)-H(1)	115.7(3) 107(5) 108.7(3) 111(5) 103(3)
5b*	N(1A)-C(4A)# O(1A)-C(1A)# O(2A)-C(3A)# O(3A)-C(12A)#	1.303(4) 1.226(4) 1.352(4) 1.436(4)	C(4A)-N(1A)-O(3A)# N(1A)-O(3A)-C(12A)# C(3A)-O(2A)-H(1AA)#	114.4(2) 108.5(2) 109(3)
6	N(1)-C(4) O(1)-C(1) O(2)-C(3) O(3)-C(11) C(2)-C(3)	1.2994(9) 1.2326(9) 1.3314(9) 1.4506(10) 1.3603(10)	C(4)-N(1)-O(3) N(1)-O(3)-C(11) C(3)-O(2)-H(2O)	116.41(7) 108.03(7) 111.1(12)

'*syn*' isomer

The ORTEP diagrams of compounds **4**, **5**, and **6** are shown in Fig. 3. The crystal data is presented in Table 3, and the selected bond distances and angles are presented in Table 4. The hydrogen bonding geometries are shown in Table S3 in ESI†. Compound **4** crystallizes in the orthorhombic space group $P2_12_12_1$, whereas **5**, **5b***, and **6** crystallize in the monoclinic space group $P2_1/C$. The oxime functional group (C=N-OMe) shows disorders in **4** and **5** from the additional Q peaks for this group due to stereoisomers in the crystal data. Two CIF files were generated from the intensity of the Q peaks, and these are assigned as major isomers designated as '**b**' (intramolecular O-H···O bonding) and minor isomers '**a**' (intramolecular O-H···N bonding) in compound **4**. The structure motifs reveal that the major isomer is a '*syn'* (**b**) isomer, and the minor isomer is an '*amphi*' (**a**) isomer in compound **4**. In contrast, in compounds **5** and **6**, the major isomer is '*amphi*' (**a**) isomer (intramolecular O-H···N bonding), and '*syn*' (**b**) (intramolecular O-H···O bonding) isomer is a minor isomer.

The bond distances of the '*amphi'* isomer of **4a** were evaluated by Mercury 3.8 software. The carbonyl bond distance of all compounds is ~ 1.23 Å and is similar to several other naphthoquinone compounds [4, 7, 39]. The C=N bond distances vary in isomers (Table 4). The '*syn*' isomer of '**4b**' is connected to six similar molecules via C-H···O and O-H···O hydrogen bonding interaction (Fig. S21 in ESI†). Four similar molecules are connected via C-H···O interaction, whereas two molecules via O-H···O hydrogen bonding interaction. The oxygen O(2) shows bifurcated hydrogen bonding with methoxy hydrogen H(11C) and benzenoid hydrogen H(7)(Fig. 4). Fig. 4 shows the polymeric chain of **4b** molecule formed through the C-H···O interaction of methoxy hydrogen (H(11C)) and quinonoid oxygen (O(2)), and two such chains are connected through O-H···O (O(1)-H(10)···O(1), -1/2+x,1/2-y,1-z) and C-H···O (C(7)-H(7A)···O(2), 2-x,-1/2+y,1/2-z) interactions.

The '*amphi*' isomer **4a** is connected to seven similar molecules via C-H···O and O-H···O hydrogen bonding interaction (Fig.S22 in ESI†). Five similar molecules are connected

via C-H···O interaction, whereas two molecules via O-H···O hydrogen bonding interaction. Hydrogens H(7) and H(8) of the benzenoid ring both take part in C-H···O interaction; this is the difference compared to isomer **4b**. There is a difference in the intramolecular hydrogen bonding in **4a** and **4b** isomers. **4b** isomer shows O-H···O, whereas **4a** isomer shows O-H···N interaction. The bond distance of C(1)-N(1) in **4b** isomer is 1.305(3) Å and for longer **4a** isomer C(1)-N(1A) is 1.35(2)Å (Table 4).

For compound **5**, the major isomer is observed as an *'amphi'* isomer and is designated as **5a**. Each molecule of isomer **5a** is in the vicinity of four similar molecules via O-H···O and C-H···O interactions. A polymeric chain of **5a** molecules is facilitated via C-H···O interaction by methoxy hydrogen and oxygen O(1) (Fig.5). The neighboring C-H···O bonded chain is in the reverse direction when viewed down the b-axis. Two such C-H···O bonded are connected via O-H···O interaction. The benzenoid and quinonoid rings are π-π stacked with a distance of ~3.875 Å (Fig. S23 in ESI†). The molecule **5b** is in the vicinity of five similar molecules. This isomer lacks the C-H···O interaction by methoxy proton (Fig.S25 in ESI†); however, the molecules show O-H···O when viewed down the b-axis.

In an attempt to synthesize Cu(II) complex of **5** in methanol, crystals of unreacted ligand are yielded in the filtrate. The crystal structure shows a predominant '*syn'* isomer (intramolecular O-H···O bonding) of **5** and is designated as **5b***. The concentration of stereoisomers of **5** in DMSO is 53:47, as revealed from ^{1}H NMR. Moreover, the conversion is facilitated by ~5 kJ mol^{-1} (supra DFT studies) of energy. Two π-π stacked molecules in the asymmetric unit 5b* differed in minor differences in bond distances and angles. The polymeric chain of **5b*** molecules is formed via C-H···O interaction, and the chains were also connected via C-H···O and π-π interactions (Fig. 6).

For compound **6**, only the *'amphi'* isomer is observed. The quinonoid carbonyl and C=N bond distances in **6** are (C(1)-O(1) = 1.2326(9)Å, N(1)-C(4) = 1.2994(9) Å) respectively

(Table 4), similar to the oxidized form of naphthoquinone and similar oximes[4, 7, 40]. Each molecule of 6 is connected to eight similar molecules via C-H···Cl, O-H···O, and C-H···O interactions (Fig.7). The oxygen O(1) shows bifurcated hydrogen bonding interaction. The intramolecular O(2)-H(20)···N(1) hydrogen bonding observed in **6** molecule. Slipped π-π stacking interaction was observed to the molecules through C(1) and C(6) (3.367(1), -1+x, y, z) to **6** molecules (Fig.S28 in ESI†).

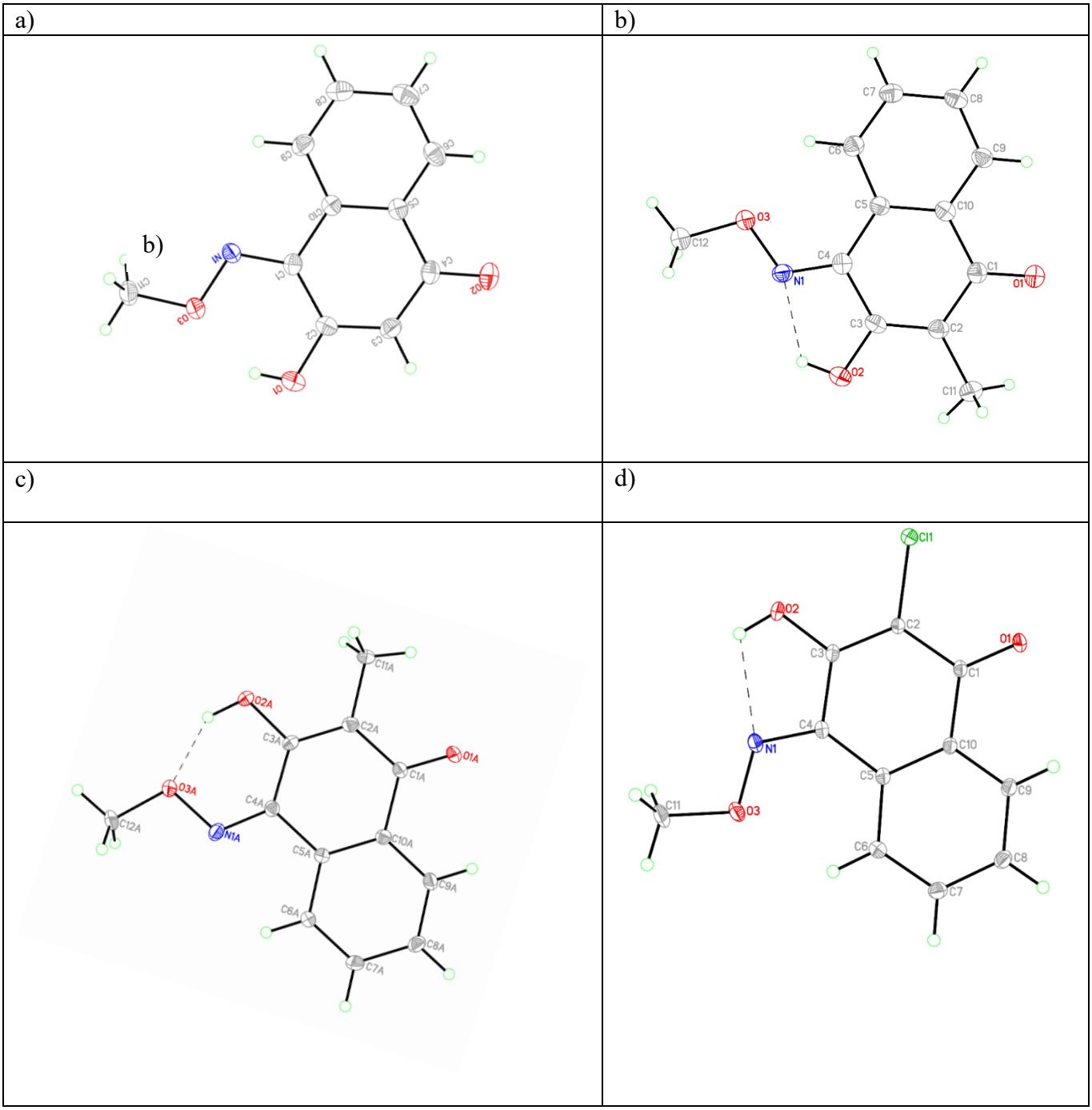

Fig. 3. ORTEP of a) **4**, b) **5**, c) **5b*** and d) **6** the ellipsoids are drawn with a 50% probability.

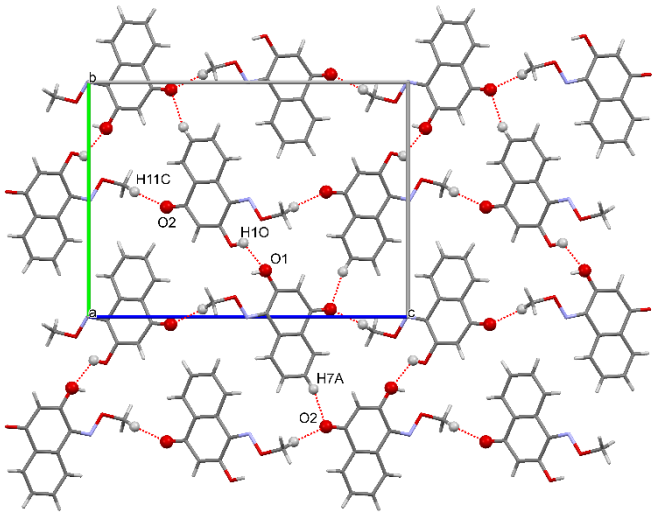

Fig. 4. Molecular packing of **4b** down c-axis.

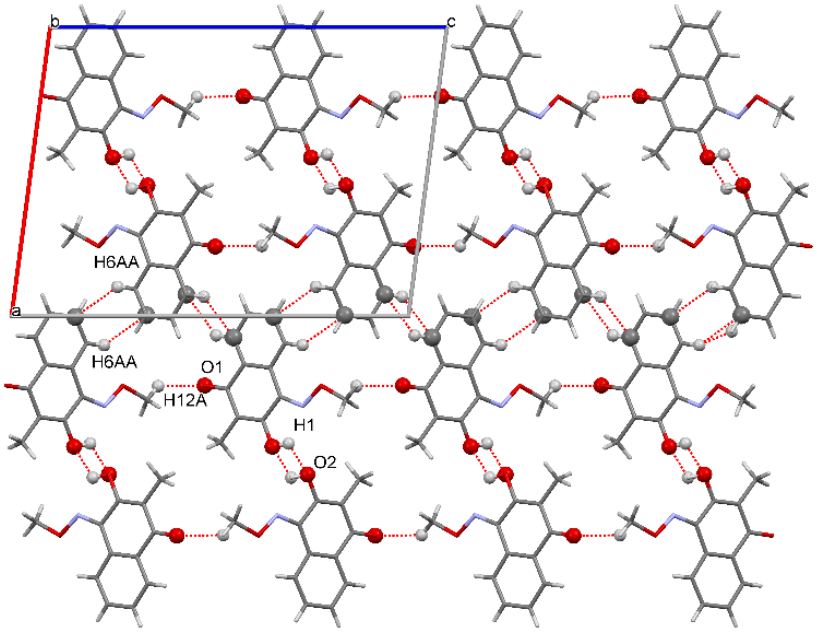

Fig. 5. Molecular packing of **5a** down the b-axis.

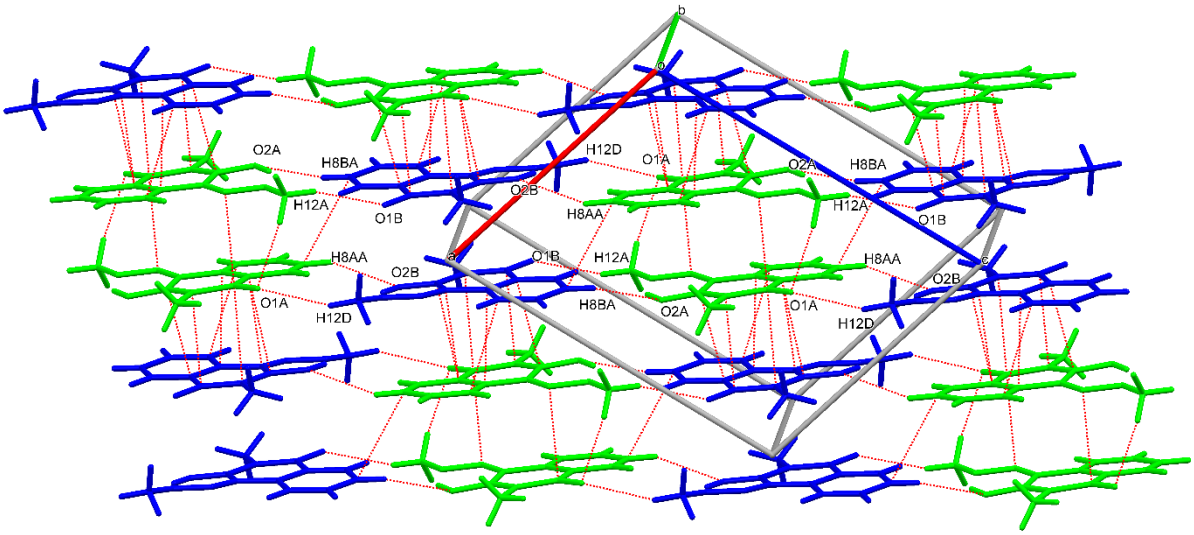

Fig. 6. Molecular packing of **5b*** down the b-axis.

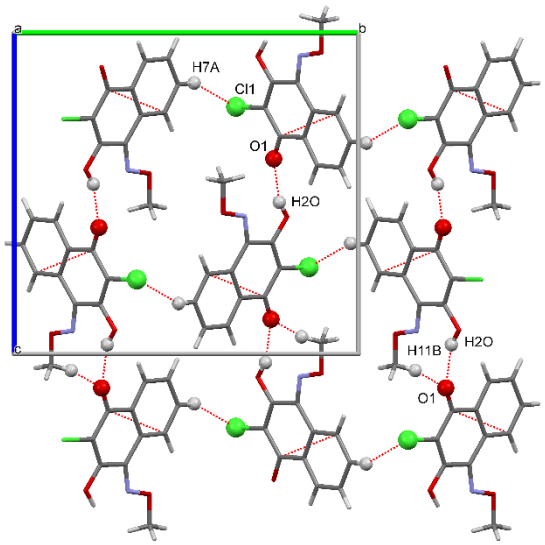

Fig. 7. Molecular packing of **6** down a-axis.

3.4. DFT Investigations

The naphthoquinone oxime ether derivatives **4**, **5**, and **6** adopt various spatial orientations of hydroxyl and methoxy groups, converging to four other structures. Optimized structures obtained from the ωB97x-D /6-311++G(d,p) theory are shown in Fig.8. The zero-point energy corrected stabilization energies relative to the lowest energy isomer are given in parentheses. As shown, the isomer **4a** turns out to be the lowest energy for **4** can be attributed to O–H···N (1.958 Å) and C–H···O (2.109 Å) interactions that engender five and six-membered rings depicted in Fig. 8. The **4b** conformer next lower in the energy order possesses O–H···O (1.723 Å) interactions only. The weaker C–H···O (2.082 Å) interactions along with N···O repulsions (separations of ~ 2.521 Å) can be inferred for the **4c** isomer, which turns out to be 19.7 kJ mol^{-1} higher in energy compared to the lowest energy isomer **4a**. Lastly, the **4d** isomer, void of the hydrogen bonding, is largely destabilized. The energy hierarchy: **4a**> **4b** > **4c** > **4d** in the case of **4** thus can be explained in terms of intramolecular interactions. Similar inferences are drawn for **5** or **6** analogues. These inferences are consistent with the earlier studies on the isomerization of naphthoquinone oximes reported in the literature [7]. Conformational isomers in naphthoquinone derivatives **4**, **5**, and **6** are portrayed in Fig.9. Selected structural parameters in the two low-lying energy isomers obtained from the present theory are reported in Table S4 in ESI†.

The ramifications of the structural attributes of different isomers to their vibrational spectra were analyzed through normal vibration analyses. Selected frequencies of salient vibrations in the two low energy isomers of **4**, **5**, and **6** are summarized in Table 1. The calculated vibrational frequencies are harmonic and are usually scaled appropriately before comparison with the experiment, as indicated in Table 1. The scaling factor (equal to 0.938) has been chosen such that the scaled frequency of the $\nu_{C=O}$ stretching vibration is congruent with the characteristic carbonyl in the observed infrared spectra of **4**, **5**, or **6**. A strong hydrogen

bonding renders ample stability to the **4a** conformer; the O-H stretching was predicted to be at 3490 cm^{-1} vibration, which is found to be 14 cm^{-1} lower wavenumber when compared with the isomer **4b**. The low-lying energy isomers in **5** and **6** led to similar inferences for the hydrogen-bonded hydroxyl vibrations.

The ^{1}H NMR chemical shifts for the two lowest energy conformers DMSO-d_6 simulated with the help of SCRF-PCM theory are compared to the experiment in Table 5. The SCRF-PCM model using DMSO-d_6 as solvent led to the hierarchy of δ_H values: H(8) > H(5) > H(7) ~ H(6) > H(3) > H(11) for the **4a** isomer, which matches pretty well with the experiment. The hydroxyl proton H(1) in the lowest energy isomers has not been included. Moreover, the C-H···O interactions in **4a** evince upfield δ_H signal at 9.42 ppm for the H(8) proton in the **4a** isomer. In comparison, the H5 proton was deshielded and showed its signal near δ 8.73 ppm owing to the electron-withdrawing carbonyl group. On the other hand, the methyl proton emerges with up-field δ_H signals (4.3 ppm) in the calculated ^{1}H NMR. The signals for H(6) and H(7) protons were predicted to be near 8.1 ppm. For the **4b** isomer, the shielding (0.77 ppm) of the H(8) proton was noticed. Similar inferences can be drawn for the isomers **5** and **6.** Calculated ^{1}H NMR chemical shifts for the two high-energy isomers have been presented in Table S2 in ESI†.

The charge distribution within the HOMO and LUMO of two low-lying energy isomers of **4**, **5**, and **6** are portrayed in Fig.9. As shown, the lowest energy isomers reveal the HOMO to be mainly residing on the quinonoid ring. At the same time, the LUMO extends over the entire molecular framework.

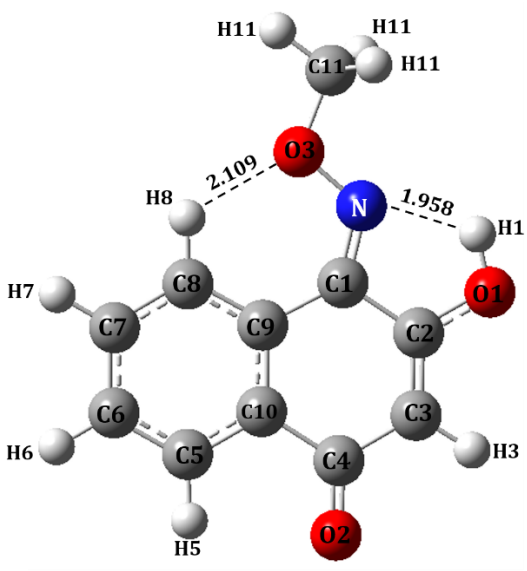

4a (0.0)

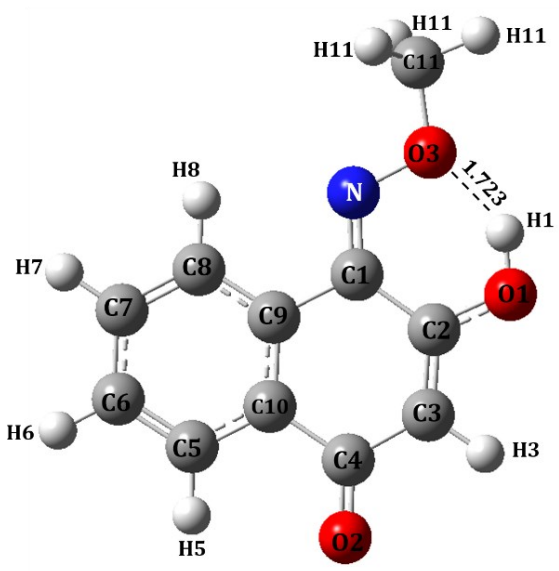

4b (5.2)

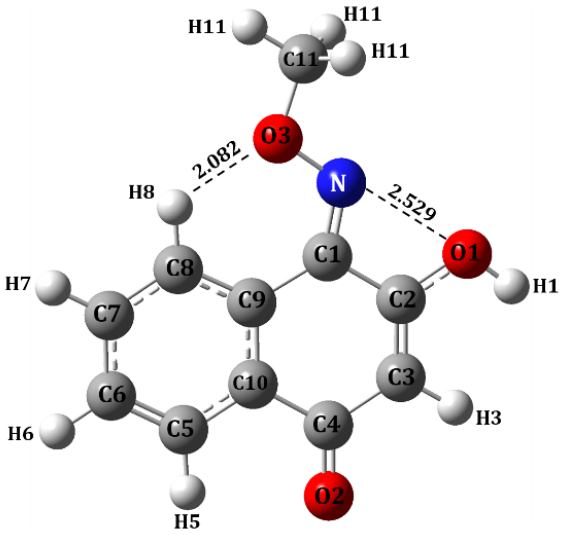

4c (19.7)

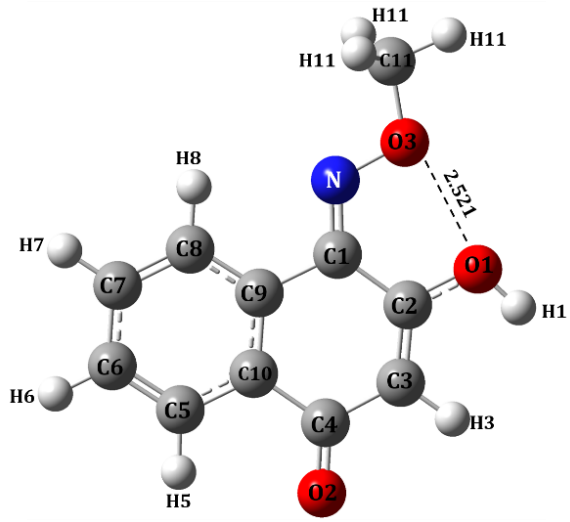

4d (30.8)

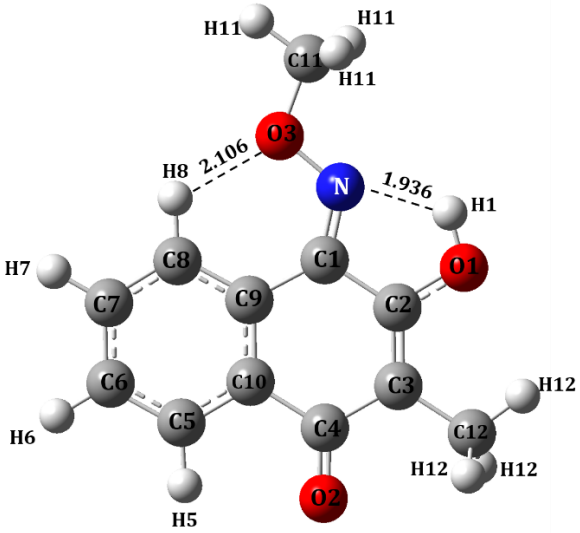

5a (0.0)

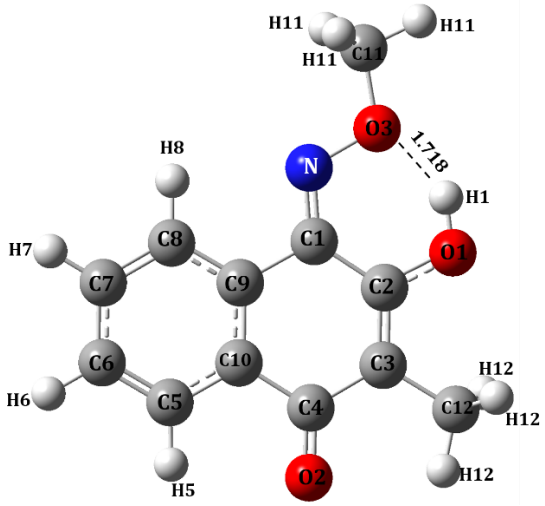

5b (5.9)

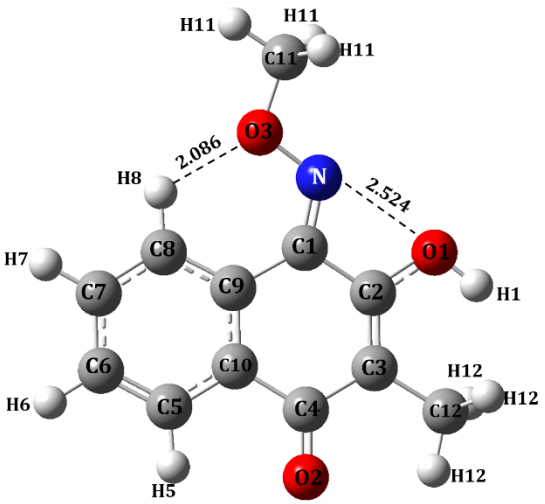

5c (26.2)

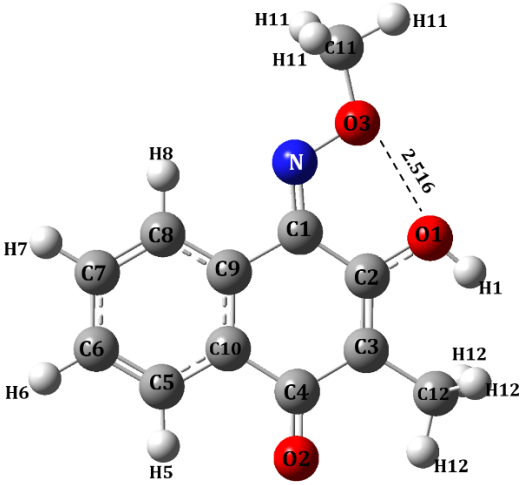

5d (31.7)

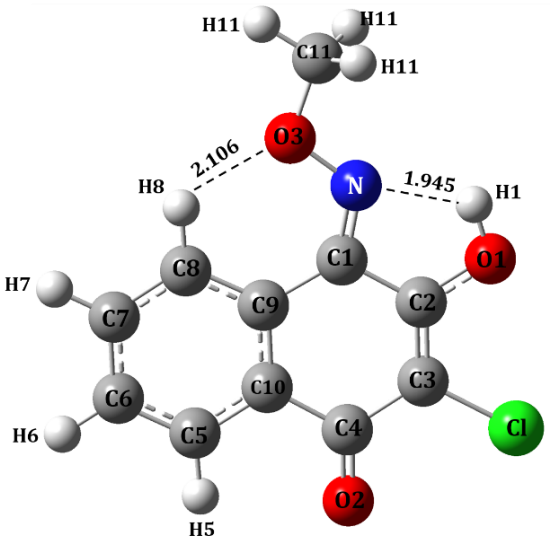

6a (0.0)

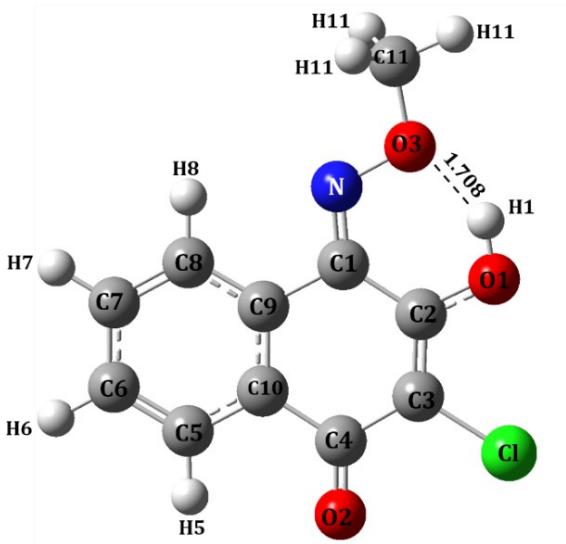

6b (4.9)

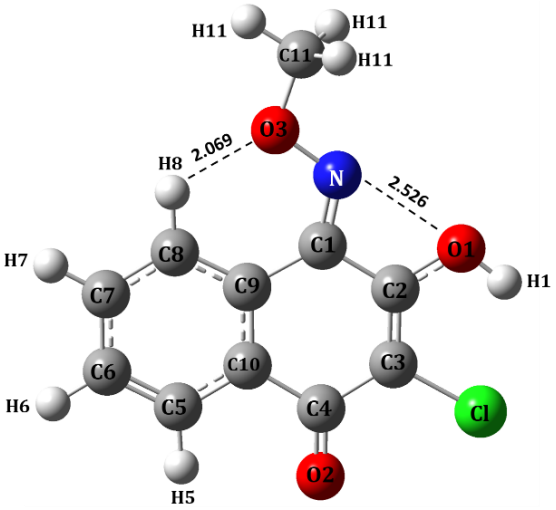

6c (11.2)

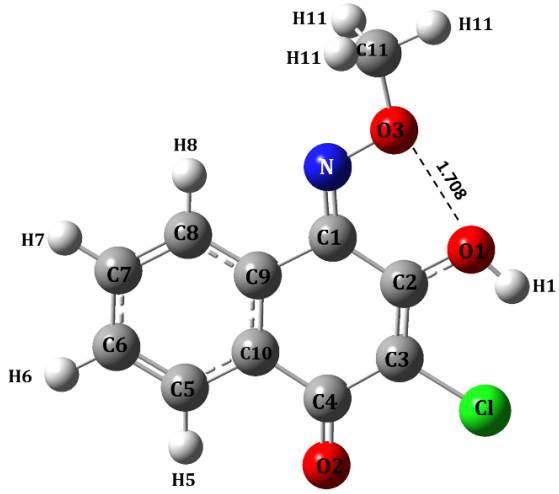

6d (16.4)

Fig. 8. Optimized Conformational isomers of naphthoquinone derivatives **4**, **5** and **6**. Numbers in parentheses denote zero point corrected relative stabilization energies (in kJ.mol^{-1}) concerning the lowest energy structure

Table 5 Comparison of ^{1}H NMR chemical shifts (ppm) values in solvent DMSO- d_6 for low energy isomers of **4**, **5**, and **6**

	4				**5**				**6**			
	4a		**4b**		**5a**		**5b**		**6a**		**6b**	
	Theory	Exp	Theory	Exp	Theory	Exp	Theory	Exp	Theory	Exp	Theory	Exp
H(1)	7.68	11.08	9.33	11.28	7.67	10.03	9.45	10.95	8.07	---	9.99	---
H(3)	6.17	5.88	6.12	5.93	---	---	---	---	---	---	---	---
H(5)	8.73	8.05	8.53	7.92	8.74	8.10	8.58	8.08	8.81	8.13	8.62	8.05
H(6)	8.07	7.65	7.97	7.56	8.04	7.79	7.94	7.84	8.09	7.71	8.00	7.56
H(7)	8.11	7.67	8.01	7.59	8.07	7.98	7.97	7.98	8.15	7.74	8.04	7.59
H(8)	9.42	8.76	8.65	7.70	9.41	8.73	8.64	8.05	9.43	8.75	8.65	7.70
H(11)	4.32 4.44	4.17	4.35 4.36	4.26	4.41 4.31	4.20	4.34 4.35	4.28	4.46 4.36	4.22	4.40	4.32
H(12)	---	---	---	---	2.48 1.83	1.91	2.74 1.76	1.94	---	---	---	---

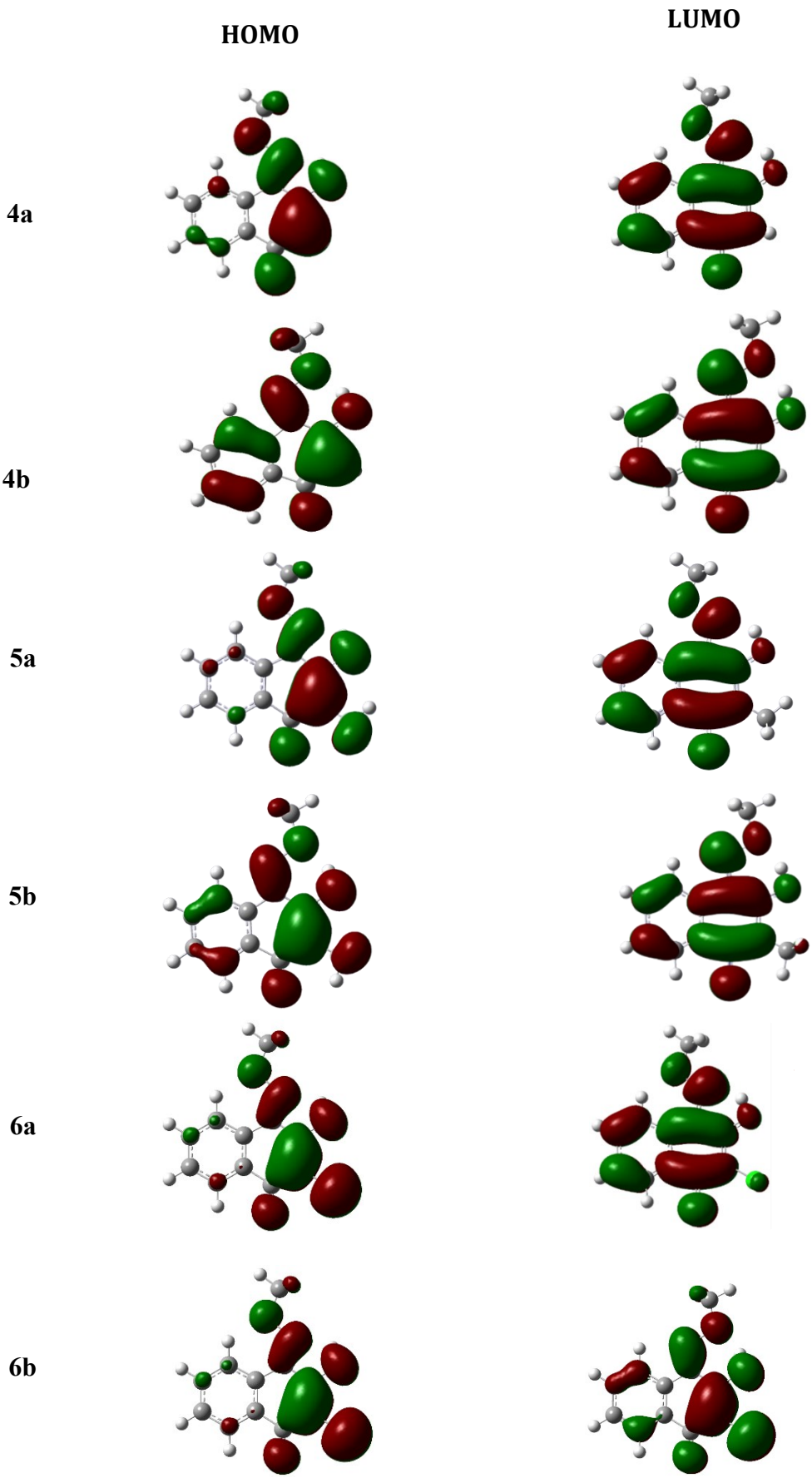

Fig. 9. Frontier molecular orbitals of lowest energy isomers of **4**, **5**, and **6**.

*3.5. Separation of 3-hydroxy-4-(methoxyimino)naphthalen-1(4H)-one (**4**) isomers*

The isomers of 3-hydroxy-4-(methoxyimino)naphthalen-1(4H)-one (**4**) were separated using a mobile phase comprising of ammonium bicarbonate and acetonitrile. Chromatographic separation is based on gradient elution. The Chromatogram obtained of **4** at pH 8.5 (Fig S20 in ESI†) shows two distinct peaks, exhibiting good resolution from each other; we designated these two peaks as isomer X and Y. Peak shape is sharp for isomer X compared to isomer Y. The peak profile of isomer Y appears broad and exhibits multiple peaks, possibly indicating the presence of *syn*, *anti*, and *amphi* isomers in the solution [3,5].

4. Conclusions

The molecular structures of naphthoquinone oxime ethers **4**, **5**, and **6** have been studied using an array of experiments, including NMR, FT-IR, MALDI, single crystal X-ray diffraction experiments combined with the ωB97x-D/6-311++G(d,p) level of density functional theory. An in-depth structural analysis of conformational isomers of these derivatives indicated the hitherto compounds represent a mixture of conformational isomers, whose energy hierarchy has largely been governed by hydrogen bonding interactions. The NMR spectral data in DMSO-d_6 showed that the '*amphi'* form is the predominant conformational isomer for **5** and **6** and *the 'syn'* form for **4**. These conclusions are further supported by the solid-state structures of all three compounds derived from single-crystal X-ray diffraction data and further backed by computations based on the density functional theory. The present endeavor furnishes molecular insights into structural and spectral characteristics of naphthoquinone oxime ether derivatives and would provide impetus for potential applications in biological applications.

†Electronic Supplementary Information (ESI) is available: Characterization of all three compounds by FTIR (Fig.S1-S3), ^{1}H NMR (Fig.S4, Fig.S6, Fig.S8), ^{13}C NMR (Fig.S5, Fig.S7, Fig.S9), COSY (Fig.S10, Fig.S12, Fig.S14 in ESI†), HSQC (Fig.S11, Fig.S13, Fig.S15 in ESI†), UV-Visible spectra (Fig.S16), MALDI-TOF (Fig.S17-S19), HPLC Chromatogram of **4** (Fig.S20), crystallography contacts and molecular packing (Fig.S21-S28), Experimental and calculated ^{13}C NMR shift values (Table S1), Calculated ^{1}H NMR chemical shift values of isomers higher in energy (Table S2) and Hydrogen bonding geometry for **4**, **5**, **5b*** and **6** (Table S3), Selected bond distances (in Å) in low-lying energy isomers of **4**, **5**, and **6** (Table S4)

Crystallographic data have been deposited with the Cambridge Crystallographic Data Centre. They may be obtained on request quoting the deposition number CCDC numbers 2298742 for **4**, 2298744 for **5**, 2329132 for **5b*** and 2298743 for **6**, from the CCDC, 12 Union Road, Cambridge CB21EZ, UK (fax: +44 1223336 033; E-mail address: deposit@ccdc.cam.ac.uk).

Author's Contribution

Vivek B. Mokashi: Conceptualization, Methodology, Data curation, Writing- Original draft.

Sunita Salunke-Gawali: Conceptualization, Review & editing, Data curation, Supervision, Methodology, Funding acquisition.

Maneesha Shewale: Methodology, Data Curation

Shridhar P. Gejji: Methodology, Data Curation**,** Review & Editing

Ray J. Butcher: Data curation

Conflicts of interest

The authors declare no conflict of interest.

Acknowledgments

VBM thanks Chhatrapati Shahu Maharaj Research, Training and Human Development Institute Pune, India, for financial support through the vide Chhantrapti Shahu Maharaj Research Fellowship-2020(CSMNRF-2020). SSG acknowledges DST-SERB, Government of India (Ref. No. EMR/2016/007912) for financial support. ChemMatCARS (for the crystal structure of **5**) Sector 15 is supported by the National Science Foundation under grant number NSF/CHE-1834750. This research used resources from the Advanced Photon Source, a U.S. Department of Energy (DOE) Office of Science User Facility operated for the DOE Office of Science by Argonne National Laboratory under Contract No. DE-AC02-06CH11357.

References

[1] M.M. Moustafa, Spectrophotometric analysis, thermal analysis and gravimetric determination of some metal ions with oxime and Schiff's base derivatives of N-furoylphenylhydroxylamine, J. Therm. Anal. 50 (1997) 463–471. https://doi.org/10.1007/BF01980506.

[2] S.Y. Rane, D.D. Dhavale, M.P. Mulay, E.M. Khan, Isomer trigger of hydroxyquinone monoximes, Spectrochim. Acta Part Mol. Spectrosc. 46 (1990) 113. https://doi.org/10.1016/0584-8539(93)80019-7.

[3] Y. Shinde, S. Sproules, L. Kathawate, S. Pal, V.B. Konkimalla, S. Salunke-Gawali, Separation and isolation of tautomers of 2-hydroxy-4-naphthoquinone-1-oxime derivatives by liquid chromatography: Antiproliferative activity and DFT studies, J. Chem. Sci. 126 (2014) 213–225. https://doi.org/10.1007/s12039-013-0549-9.

[4] Y. Shinde, R. Patil, V. Badireenath Konkimalla, S.B. Merugu, V. Mokashi, S. Harihar, J. Marrot, R.J. Butcher, S. Salunke-Gawali, Keto-enol tautomerism of hydroxynaphthoquinoneoxime ligands: Copper complexes and topoisomerase inhibition activity, J. Mol. Struct. 1262 (2022) 133081. https://doi.org/10.1016/j.molstruc.2022.133081.

[5] Y. Shinde, S. Salunke-Gawali, Reversed phase chromatographic separation and isolation of tautomers of naphthoquinoneoximes by HPLC. Effect of ph of mobile phase on separation of 3-chloro-2-hydroxy-4-naphthoquinone-1-oxime, J. Anal. Chem. 69 (2014) 1171–1178. https://doi.org/10.1134/S1061934814120144

[6] S. Bhand, R. Patil, Y. Shinde, D.N. Lande, S.S. Rao, L. Kathawate, S.P. Gejji, T. Weyhermüller, S. Salunke-Gawali, Tautomerism in o-hydroxyanilino-1,4-naphthoquinone derivatives: Structure, NMR, HPLC, and density functional theoretical investigations, J. Mol. Struct. 1123 (2016) 245–260. https://doi.org/10.1016/j.molstruc.2016.06.026.

[7] D.R. Thube, A.V. Todkary, K.A. Joshi, S.Y. Rane, S.P. Gejji, S.A. Salunke, J. Marrot, F. Varret, Theoretical and experimental investigations on the structure and vibrational spectra of 2-hydroxy-3-methyl-1,4-naphthoquinone-1-oxime, J. Mol. Struct. THEOCHEM. 622 (2003) 211–219. https://doi.org/10.1016/S0166-1280(02)00646-2.

[8] S. Ghasemzadeh, J.A. Qureshi, Demographic analysis of fenpyroximate and thiacloprid exposed predatory mite Amblyseius swirskii (Acari: Phytoseiidae), PLOS ONE. 13 (2018) e0206030. https://doi.org/10.1371/journal.pone.0206030

[9] B. Chakravarti, T. Akhtar, B. Rai, M. Yadav, J. Akhtar Siddiqui, S.K. Dhar Dwivedi, R. Thakur, A.K. Singh, A.K. Singh, H. Kumar, K. Khan, S. Pal, S.K. Rath, J. Lal, R. Konwar, A.K.

Trivedi, D. Datta, D.P. Mishra, M.M. Godbole, S. Sanyal, N. Chattopadhyay, A. Kumar, Thioaryl Naphthylmethanone Oxime Ether Analogs as Novel Anticancer Agents, J. Med. Chem. 57 (2014) 8010–8025. https://doi.org/10.1021/jm500873e

[10] H.T. Nguyen, Q.G. Nguyen Thi, T.H. Nguyen Thi, P.H. Thi, G. Le-Nhat-Thuy, T.A. Dang This, B. Le-Quang, H. Pham-The, T. Van Nguyen, Synthesis and biological activity, and molecular modeling studies of potent cytotoxic podophyllotoxin-naphthoquinone compounds, RSC Adv. 12 (2022) 22004–22019. https://doi.org/10.1039/D2RA03312G.

[11] K. Bhandari, N. Srinivas, G.B. Shiva Keshava, P.K. Shukla, Tetrahydronaphthyl azole oxime ethers: The conformationally rigid analogues of oxiconazole as antibacterials☆, Eur. J. Med. Chem. 44 (2009) 437–447. https://doi.org/10.1016/j.ejmech.2008.01.006

[12] R. Xia, T. Guo, M. Chen, S. Su, J. He, X. Tang, S. Jiang, W. Xue, Synthesis, antiviral and antibacterial activities and action mechanism of penta-1,4-dien-3-one oxime ether derivatives containing a quinoxaline moiety, New J. Chem. 43 (2019) 16461–16467. https://doi.org/10.1039/C9NJ03019K.

[13] S.H. Cardoso, C.R. De Oliveira, A.S. Guimarães, J. Nascimento, J. De Oliveira Dos Santos Carmo, J.N. De Souza Ferro, A.C. De Carvalho Correia, E. Barreto, Synthesis of newly functionalized 1,4-naphthoquinone derivatives and their effects on wound healing in alloxan-induced diabetic mice, Chem. Biol. Interact. 291 (2018) 55–64. https://doi.org/10.1016/j.cbi.2018.06.007.

[14] A. Rossello, S. Bertini, A. Lapucci, M. Macchia, A. Martinelli, S. Rapposelli, E. Herreros, B. Macchia, Synthesis, Antifungal Activity, and Molecular Modeling Studies of New Inverted Oxime Ethers of Oxiconazole, J. Med. Chem. 45 (2002) 4903–4912. https://doi.org/10.1021/jm020980t.

[15] S. Tu, Y.-Q. Xie, S.-Z. Gui, L.-Y. Ye, Z.-L. Huang, Y.-B. Huang, L.-M. Che, Synthesis and fungicidal activities of novel benzothiophene-substituted oxime ether strobilurins, Bioorg. Med. Chem. Lett. 24 (2014) 2173–2176. https://doi.org/10.1016/j.bmcl.2014.03.024.

[16] M.I. El-Gamal, S.M. Bayomi, S.M. El-Ashry, S.A. Said, A.A.-M. Abdel-Aziz, N.I. Abdel-Aziz, Synthesis and anti-inflammatory activity of novel (substituted)benzylidene acetone oxime ether derivatives: Molecular modeling study, Eur. J. Med. Chem. 45 (2010) 1403–1414. https://doi.org/10.1016/j.ejmech.2009.12.041.

[17] M.R. Gannarapu, S.B. Vasamsetti, N. Punna, N.K. Royya, S.R. Pamulaparthy, J.B. Nanubolu, S. Kotamraju, N. Banda, Synthesis of novel 1,2-benzothiazine 1,1-dioxide-3-methanone

oxime N-aryl acetamide ether derivatives as potent anti-inflammatory agents and inhibitors of monocyte-to-macrophage transformation, Eur. J. Med. Chem. 75 (2014) 143–150. https://doi.org/10.1016/j.ejmech.2013.12.053.
[18] H.-J. Park, K. Lee, S.-J. Park, B. Ahn, J.-C. Lee, H. Cho, K.-I. Lee, Identification of antitumor activity of pyrazole oxime ethers, Bioorg. Med. Chem. Lett. 15 (2005) 3307–3312. https://doi.org/10.1016/j.bmcl.2005.03.082.
[19] A.D. Latif, T. Gonda, M. Vágvölgyi, N. Kúsz, Á. Kulmány, I. Ocsovszki, Z.P. Zomborszki, I. Zupkó, A. Hunyadi, Synthesis and In Vitro Antitumor Activity of Naringenin Oxime and Oxime Ether Derivatives, Int. J. Mol. Sci. 20 (2019) 2184. https://doi.org/10.3390/ijms20092184
[20] F. Delmas, M. Gasquet, P. Timon-David, N. Madadi, P. Vanelle, A. Vaille, J. Maldonado, Synthesis and in vitro anti-protozoan activity of new 5-nitrothiophene oxime ether derivatives, Eur. J. Med. Chem. 28 (1993) 23–27. https://doi.org/10.1016/0223-5234(93)90075-P.
[21] Z. Mirjafary, M. Abdoli, H. Saeidian, S. Boroon, A. Kakanejadifard, Oxime ethers as versatile precursors in organic Synthesis: a review, RSC Adv. 5 (2015) 79361–79384. https://doi.org/10.1039/C5RA15299B.
[22] Z. Mirjafary, M. Abdoli, H. Saeidian, A. Kakanejadifard, S.M.F. Farnia, Review of the Synthesis of acyclic and cyclic oxime ethers, RSC Adv. 6 (2016) 17740–17758. https://doi.org/10.1039/C5RA25591K
[23] S. Choi, S. Ha, C.-M. Park, α-Diazo oxime ethers for N-heterocycle synthesis, Chem. Commun. 53 (2017) 6054–6064. https://doi.org/10.1039/C7CC02650A.
[24] H. Miyabe, M. Ueda, N. Yoshioka, K. Yamakawa, T. Naito, Reactions of Alkyl Radicals with Oxime Ether: One-Pot Synthesis of α-Amino Acids, Tetrahedron. 56 (2000) 2413–2420. https://doi.org/10.1016/S0040-4020(00)00119-8.
[25] I. Bozbey, H. Uslu, B. Türkmenoğlu, Z. Özdemir, A. Karakurt, S. Levent, Conventional and microwave prompted Synthesis of aryl(alkyl)azole oximes, 1H-NMR spectroscopic determination of E/Z isomer ratio and HOMO-LUMO analysis, J. Mol. Struct. 1251 (2022) 132077. https://doi.org/10.1016/j.molstruc.2021.132077.
[26] Y. Kaya, V.T. Yilmaz, T. Arslan, O. Buyukgungor, Experimental and theoretical DFT studies of structure, spectroscopic and fluorescence properties of a new imine oxime derivative, J. Mol. Struct. 1024 (2012) 65–72. https://doi.org/10.1016/j.molstruc.2012.05.032.
[27] E. Sánchez-Pavón, S. Rosete-Luna, R. Colorado-Peralta, M.F. Hernández-Hernández, M. Sánchez, A. Flores-Parra, Ó. García-Barradas, D. Hernández-Romero, Spectroscopic and computational analysis of the (E/Z)-isomers in synthesizing new alkyl-oxime derivatives, J.

Mol. Struct. 1219 (2020) 128563. https://doi.org/10.1016/j.molstruc.2020.128563.
[28] J. Das, C.V.L. Rao, T.V.R.S. Sastry, M. Roshaiah, P.G. Sankar, A. Khadeer, M.S. Kumar, A. Mallik, N. Selvakumar, J. Iqbal, S. Trehan, Effects of positional and geometrical isomerism on the biological activity of some novel oxazolidinones, Bioorg. Med. Chem. Lett. 15 (2005) 337–343. https://doi.org/10.1016/j.bmcl.2004.10.073.
[29] G. Yao, M. Muhammad, J. Zhao, J. Liu, Q. Huang, DFT-based Raman spectral study of astaxanthin geometrical isomers, Food Chem. Mol. Sci. 4 (2022) 100103. https://doi.org/10.1016/j.fochms.2022.100103.
[30] S. Salunke-Gawali, L. Kathawate, V.G. Puranik, MOF with hydroxynaphthoquinone as organic linker: Molecular structure of [Zn(Chlorolawsone)$_2$(H2O)$_2$] and thermogravimetric studies, J. Mol. Struct. 1022 (2012) 189–196. https://doi.org/10.1016/j.molstruc.2012.05.012.
[31] L. Kathawate, S. Sproules, O. Pawar, G. Markad, S. Haram, V. Puranik, S. Salunke-Gawali, Synthesis and molecular structure of a zinc complex of the vitamin K3 analog phthiocol, J. Mol. Struct. 1048 (2013) 223–229. https://doi.org/10.1016/j.molstruc.2013.05.057.
[32] G. M. Sheldrick. SADABS, Brucker-Siemens Area Detector Absorption and Other Correlation. University of Gottingen, Germany, 2006 Version 2008/1.
[33] G. M. Sheldrick, SHELX-97 Program for Crystal Structure Solution and Refinement, University of Gottingen, Germany. 1997.
[34] M. J. Frisch, G. W. Trucks, H. B. Schlegel, G. E. Scuseria, M. A. Robb, J. R. Cheeseman, G. Scalmani, V. Barone, B. Mennucci, G. A. Petersson, H. Nakatsuji, M. Caricato, X. Li, H. P. Hratchian, A. F. Izmaylov, J. Bloino, G. Zheng, J. L. Sonnenberg, M. Hada, M. Ehara, K. Toyota, R. Fukuda, J. Hasegawa, M. Ishida, T. Nakajima, Y. Honda, O. Kitao, H. Nakai, T. Vreven, J. A. Montgomery Jr., J. E. Peralta, F. Ogliaro, M. Bearpark, J. J. Heyd, E. Brothers, K. N. Kudin, V. N. Staroverov, R. Kobayashi, J. Normand, K. Raghavachari, A. Rendell, J. C. Burant, S. S. Iyengar, J. Tomasi, M. Cossi, N. Rega, J. M. Millam, M. Klene, J. E. Knox, J. B. Cross, V. Bakken, C. Adamo, J. Jaramillo, R. Gomperts, R. E. Stratmann, O. Yazyev, A. J. Austin, R. Cammi, C. Pomelli, J. W. Ochterski, R. L. Martin, K. Morokuma, V. G. Zakrzewski, G. A. Voth, P. Salvador, J. J. Dannenberg, S. Dapprich, A. D. Daniels, O. Farkas, J. B. Foresman, J. V. Ortiz, J. Cioslowski and D. J. Fox, Gaussian 16, Revision A. 03, Gaussian, Inc., Wallingford CT, 2016.
[35] G.A. Petersson, A. Bennett, T.G. Tensfeldt, M.A. Al-Laham, W.A. Shirley, J. Mantzaris, J. Chem. Phys. 89 (1988) 2193–2218.
https://doi.org/10.1063/1.455064

[36] K. Wolinski, J.F. Hinton, P. Pulay, Efficient implementation of the gauge-independent atomic orbital method for NMR chemical shift calculations, J. Am. Chem. Soc. 112 (1990) 8251–8260. https://doi.org/10.1021/ja00179a005

[37] S.Y. Rane, E.M. Khan, Ah. Khursheed, S. Salunke-Gawali, Ligand Induced Stereoisomers Revealed in Copper(II) Complex of Nitrolawsone Oxime: EPR and Electronic Spectral Studies, Synth. React. Inorg. Met.-Org. Nano-Met. Chem. 35 (2005) 343–353. https://doi.org/10.1081/SIM-200059192.

[38] S. B. Jagtap, R. C. Chikate, O. S. Yemul, R. S. Ghadage, B. A. Kulkarni, Thermal, spectral and magnetic properties of 2-hydroxy-1,4-naphthoquinone monooximates of Ho(III), Er(III) and Yb(III), J. Therm. Anal. Calorim. 78 (2004) 251-262.

[39] K. A. Joshi, D. R. Thube, S. Y. Rane, S. P. Gejji, Ab initio and density functional studies on the structure and vibrational spectra of 2-hydroxy-1,4-naphthoquinone-1-oxime derivatives, Theor. Chem. Acc. 110 (2003) 322-327. DOI:10.1007/s00214-003-0480-0

[40] S. B. Zaware, R. G. Gonnade, D. Shrinivas, A. Khan, S. Y. Rane, Antioxidant and anticancer activities of supramolecularly controlled magnetostructural halo-oximes of lawsone, New J. Chem. 35 (2011) 1615-1623. https://doi.org/10.1039/C1NJ20176J